*Materials Transactions*, Vol. 44, No. 7 (2003) pp. 1448 to 1456

EXPRESS REGULAR ARTICLE

# A Model of the $\beta$-AlFeSi to $\alpha$-Al(FeMn)Si Transformation in Al–Mg–Si Alloys

Niels C. W. Kuijpers[1], Fred J. Vermolen[2], Kees Vuik[2] and Sybrand van der Zwaag[1,3]

[1]*Netherlands Institute for Metals Research (NIMR), Delft, 2628 AL 137, The Netherlands*
[2]*Department of Applied Mathematics, Delft University of Technology, Delft, 2628 CD 4, The Netherlands*
[3]*Department of Aerospace Engineering, Delft University of Technology, Delft, 2629 HS 1, The Netherlands*

During the homogenisation process of Al–Mg–Si extrusion alloys, plate-like $\beta$-$Al_5FeSi$ particles transform to multiple rounded $\alpha$-$Al_{12}(FeMn)_3Si$ particles. The rate of this $\beta$ to $\alpha$ transformation determines the time which is required to homogenise the aluminium sufficiently for extrusion. In this paper, a finite element approach is presented which model the development of fraction transformed with time, in the beginning of the transformation, as a function of homogenisation temperature, as-cast microstructure and concentration of alloying elements. We treat the $\beta$ to $\alpha$ transformation mathematically as a Stefan problem, where the concentration and the position of the moving boundaries of the $\alpha$ and $\beta$ particles are determined. For the boundary conditions of the model thermodynamic calculations are used (Thermo-Calc). The influence of several process parameters on the modelled transformed fraction, such as the temperature and initial thickness of the $\beta$ plates, are investigated. Finally the model is validated with experimental data.

(Received March 7, 2003; Accepted May 16, 2003)

***Keywords:*** *phase transformation, intermetallics, aluminium alloy, diffusion, homogenisation, Stefan problem*

## 1. Introduction

The phase transformation of $\beta$-AlFeSi to $\alpha$-Al(FeMn)Si is an important process during the homogenisation of cast AA 6xxx aluminium alloys. During this homogenisation process, at temperatures between 530–600°C,[1)] plate-like monoclinic intermetallic $\beta$-$Al_5FeSi$ particles transform to multiple rounded $\alpha$-$Al_{12}(Fe_xMn_{(1-x)})_3Si$ particles.[2–4)] This phase transformation improves the processability of the aluminium considerably. The plate-like $\beta$-particles can lead to local crack initiation and induce surface defects on the extruded material. The more rounded $\alpha$-particles in the homogenised material improve the extrudability of the material and improve the surface quality of the extruded material.[5,6)] Additional processes, such as the dissolution of $Mg_2Si$ particles also occur during homogenisation. Since the $Mg_2Si$ particles dissolve rather quickly, the $\beta \rightarrow \alpha$ transformation kinetics determine the minimum time which is needed to get a good extrudability.[7)] Many process parameters, such as homogenisation temperature,[8)] as-cast microstructure,[9)] and chemical compostion[10)] influence the transformation rate.

The morphological change of the intermetallics during the homogenisation treatment has been described in a few papers. In the early stage of transformations it was found that $\alpha$ particles were nucleated on top and also on the rim of the $\beta$-plate.[11,12)] Small $\alpha$ nuclei, with an average size of half a micrometer, are observed on top of the $\beta$ particles with a site density of approximately $0.2\,\mu m^{-2}$. Some of the particles observed were facetted whereas others exhibited a more rounded morphology. During the transformation, the $\beta$-AlFeSi phase is observed to remain plate-like with an approximately constant thickness,[4)] leading to the conclusion that the $\beta$ plate only dissolves at the rim, injecting Fe and Si into the Al-matrix. At a later stage of the transformation, the $\alpha$ particles will grow as spheres with possibly fingering as a side-effect.[4)] From TEM and SEM experiments, it is observed that the interface between the $\alpha$-particle and $\beta$-plate, does not move.[13)] Hence, there is no mass transport across the interface between the $\alpha$-particle and $\beta$-plate. Since the $\alpha$ particles grow by adsorption of Si, Mn and/or Fe, those elements must have been transported through the Al-matrix.

Until now, no physically based models have been found in the literature which predict the fraction transformed of the $\beta$ to $\alpha$ transformation. Hence, modelling this transformation and looking at the influence of the process parameters poses a new challenge.

The $\beta$ to $\alpha$ transformation can be mathematically treated as a Stefan problem,[14)] where the concentration satisfying the diffusion equation and the position of the moving boundaries of the $\alpha$ and $\beta$ particles are determined. The model is based on the conservation of mass. Some papers that study particle dissolution and growth by determination of the solution of a Stefan problem are due to, among many others, Whelan,[15)] Aaron and Kotler,[16)] and Tundal and Ryum.[17)] In these papers it is assumed that the interface moves due to diffusion of one alloying element only, *i.e.* binary alloys. Furthermore these models are restricted to one space dimension and one moving interface. During the $\beta$ to $\alpha$ transformation which is studied here, the interface movement is derived by the simultaneous diffusion of several alloying elements with two moving interfaces. This gives a "vector-valued" Stefan problem, where the concentration fluxes of consecutive alloying elements are such that all the alloying elements are conserved. This is explained in more detail by Reiso *et al.*,[18)] Hubert,[19)] Vitek *et al.*[20)] and Vermolen *et al.*[21,22)] The ideas from the model of Vermolen,[22)] are used to obtain the boundary conditions of the alloying elements at the interfaces.

A different numerical approach for the $\beta$ to $\alpha$ transformation is the phase-field approach, which is derived form a minimisation of the free energy functional. This approach has been used by Kobayashi[23)] to simulate dendrite growth. A recent extension to multi-component alloys phase-field computation has been done by Grafe *et al.*,[24)] where solidification and solid state transformation are modelled. However, a disadvantage of the phase-field approach is that physically justifiable parameters in the energy functional are

not easy to obtain. Some of these quantitatives have to be obtained by using fitting procedures that link experimental and numerical computations.

In this paper, a model is proposed based on the hypothesis that the transformation is diffusion controlled. This model can only be used in the beginning of the transformation. The reasons for this are: firstly, in the beginning the overall morphology is still stable, whereas the intermetallics break up to cylindrical shapes at later stages. Secondly, if the dissolving $\beta$-rim meets the growing $\alpha$-particle, our model is no longer applicable. Despite this limitation, the model could provide some idea of the homogenisation-time towards higher fractions (up to ~50%).

In this paper, a finite element is presented which model the development of fraction transformed with time, by simulating the growth of an $\alpha$ particle on a $\beta$ plate. For the boundary conditions of the model thermodynamic calculations are used (Thermo-Calc). The transformation fraction is calculated for several input parameter values estimated from experimental observations. The influence of some process parameters on the transformed fraction, such as the temperature and initial thickness of the $\beta$ plates, are investigated. Finally the model is validated with experimental data. The dependence of the transformation rate on the alloy content is also an important extension of the model, and will be described in more detail in 25).

## 2. The Model

### 2.1 Introduction

The as-cast microstructure is simplified in the Finite Element Model to a representative cell containing the Al-rich phase, a single $\alpha$ particle and a single $\beta$-plate, which have a specific form and size. Furthermore, the cell-size is chosen such that diffusion across cell-boundaries is negligible. Both a uniform and a spatially graded initial (at $t = 0$) composition in the Al-rich phase can be assumed. For the present study only a uniform initial composition of the Al-rich phase is considered. It is assumed that the atoms of the alloying elements diffuse through the Al-rich phase. Further, atoms that originate from the $\alpha$- and $\beta$-phase are assumed to cross the interface ($\alpha$/Al phase or $\beta$/Al phase) at such a rate that bulk diffusion is the rate controlling step in the transformation. For clarity, we list the assumptions that we use to predict the rate of the $\beta \rightarrow \alpha$ transformation.

*Main assumptions of model:*

1. Diffusion determines the rate of transformation, from mass-conservation a Stefan problem results to determine the displacement of the interfaces.
2. During the growth of the $\alpha$ particle chemical elements Fe, Mn, Si cross the $\alpha$/Al interface. The $\beta$-plate only dissolves at the rim of the plate, hence the thickness of the $\beta$ plate is constant during the transformation.
3. The initial concentrations of the alloying elements Fe, Mn, Si in the aluminium matrix surrounding the intermetallics (but not at interface itself), are determined by the Scheil solidification model.[26)]
4. The interface concentrations for Fe, Mn, Si are estimated by the use of the multi-component model of Vermolen *et al.*[22)] for particle dissolution. The key assumption here is that the interface concentration of the different elements should satisfy the thermodynamic solubility relations and be such that the prediction of the interface displacement of a phase is equal for all chemical elements. This procedure is applied to both the interface of the $\alpha$-particle and $\beta$-plate.
5. In the transformation model only diffusion of Fe is taken into account with the use of the boundary conditions as given in item 4. The difference between the chemical potentials of the Fe concentration on the $\alpha$ and $\beta$ interface provides the rate limiting driving force of the $\beta \rightarrow \alpha$ transformation.
6. The concentration of Si is uniform in the Al matrix during the entire transformation.

The rate of the transformation is assumed to be determined by diffusion of Fe (See assumption 5). It is known from experiments, that during the transformation Mn is also absorbed by the $\alpha$ particles. The Mn is supplied by the dissolved Mn in the Al-matrix, and is not supplied from the $\beta$-AlFeSi. Since the diffusion of Mn is slower than that of Fe, the Mn content stays constant in the early stages of the transformation. Hence the thermodynamic solubility of iron at the rim of the $\alpha$ particle is not affected. Therefore this Mn diffusion is only a secondary effect of the transformation, and hardly controls the rate of the transformation, which was also found by Alexander *et al.* for familiar phase transformations.[27)] Therefore, in this model, the diffusion of Mn is neglected. The diffusion of Si is very fast,[28)] in comparison to diffusion of Fe, and therefore the silicon concentration will be distributed uniformly in the aluminium matrix rapidly (as stated in assumption 6).

We assume that the stoichiometry of both the $\alpha$-phase and $\beta$-phase is constant at all stages of the transformation process. Further we neglect a potential Mn concentration in the $\alpha$-particle, $Al_{12}(Fe_xMn_{1-x})_3Si$, hence $x = 1$.

### 2.2 Solubility relations of Fe on the α and the β particles

The driving force of the diffusional $\beta \rightarrow \alpha$ transformation is mainly determined by the difference between the chemical potentials of iron at the $\alpha$- and $\beta$-interface.

$$\Delta\mu = \mu_\beta^s - \mu_\alpha^s. \tag{1}$$

This difference in chemical potential, $\Delta\mu$, of the solute iron in the Al-phase close to the $\alpha(\mu_\alpha^s)$ and the $\beta$ interface $(\mu_\beta^s)$, gives a diffusional transport of iron atoms towards the $\alpha$-phase in the aluminium matrix. It is assumed that the interfacial reactions for the $\alpha$- and $\beta$-phases are fast enough to reach a local thermodynamic equilibrium concentration in both aluminium/intermetallic interfaces. The chemical potential of Fe depends on the solute levels of other elements, such as Si and Mn, at the interface.

Since the model is based on Fick's law of diffusion (see also assumption 1), we use the differences of solute level between the $\alpha$ and $\beta$ phases ($\Delta c_{Fe}$) as the driving force. Therefore, we use the thermodynamic software package Thermo-Calc (database TTAL for aluminium) to derive a relation between the equilibrium concentrations of the alloying elements at both the $\alpha$- and $\beta$-interface.

Then, it is possible to estimate the interface concentrations

on the interface of the $\alpha$ particle. For the investigated alloy composition in this study with high Mn content, a low iron equilibrium concentration at the interface was calculated (<0.005 mass%) and therefore, the iron concentration on the $\alpha$ boundary was set to $c^{\mathrm{s}}_{\alpha} = 0$ mass% for all calculations. At lower alloy concentrations of Mn (<0.015 mass%) a considerable increase of the solubility was found. In this case it is necessary to take the iron solubility on the $\alpha$ particle into account. The effect of Mn on the transformation rate will be described by Kuijpers *et al.*[25]

To compute the interface concentration for the $\beta$-plate, the solubility product is determined from Thermo-Calc for several temperatures and expressed in an Arrhenius-relation:

$$c^{\mathrm{s}}_{\beta\mathrm{Fe}} c^{\mathrm{s}}_{\beta\mathrm{Si}} = A_{\beta} \exp\left(\frac{-Q_{\beta}}{RT}\right). \tag{2}$$

Here $c^{\mathrm{s}}_{\beta\mathrm{Fe}}$ and $c^{\mathrm{s}}_{\beta\mathrm{Si}}$ are the equilibrium concentrations (in mass%) in the matrix on the interface of the $\beta$ particle, $A_{\beta} = 59 \cdot 10^3$ and $Q_{\beta} = 111$ kJ/mol. We derive an implicit relation for the initial interfacial concentration of the $\beta$-$Al_5FeSi$ in the matrix:[21]

$$\frac{c^0_i - c^{\mathrm{s}}_i}{c^{\mathrm{p}}_i - c^{\mathrm{s}}_i} \sqrt{\frac{D_i}{\pi}} \frac{\exp\left(-\dfrac{k^2}{4D_i}\right)}{\operatorname{erfc}\left(\dfrac{k}{2\sqrt{D_i}}\right)} = \frac{k}{2}, \quad \text{for} \quad i \in \{\mathrm{Si}, \mathrm{Fe}\}, \tag{3}$$

where $k$ is a constant. In eq. (3) the $c^0_i$, $c^{\mathrm{p}}_i$ and $D_i$ are the initial concentration in the matrix (mass%), concentration in the particle (mass%), and diffusion coefficient in the Aluminium matrix of element $i$. The parameter $k$ originates from the solution structure for particle dissolution/growth in a planar unbounded domain.[21] It represents the rate parameter where $S(t) = S_0 + k\sqrt{t}$ defines the interface position as a function of time. Equations (2) and (3) give sufficient conditions for the determination of $c^{\mathrm{s}}_{\mathrm{Fe}}$, $c^{\mathrm{s}}_{\mathrm{Si}}$ and $k$. The relation (3) gives the exact solution for the interface concentrations at the initial stages, for different geometries. It is assumed that the interface concentrations on the $\beta$-AlFeSi phase are constant in time and are equal to this initial interface concentration. The obtained $c^{\mathrm{s}}_{\mathrm{Fe}}$ is used as a boundary condition for the $\beta$-phase in the calculations. Since $D_{\mathrm{Si}} \gg D_{\mathrm{Fe}}$, it follows from eq. (3) that $c^{\mathrm{s}}_{\mathrm{Si}} \approx c^0_{\mathrm{Si}}$.

### 2.3 Geometry of model

For 6xxx alloys the $\alpha$ phase is stable with respect to the $\beta$ phase. The nucleation of $\alpha$-particles take place preferentially on the $\beta$/Al interface rather than in the aluminium matrix, since the activation energy for nucleation of $\alpha$ particles on the $\beta$/Al interface is lower[29] than the nucleation energy in the Al-matrix. Therefore our model considers only this heterogeneous nucleation of $\alpha$-particles on the $\beta$/Al surface. Experimentally, a distribution of nucleation distances was found, but for the sake of simplicity we only take the mean nucleation distance as model input parameter.

The average plate length of the initial $\beta$-particles is approximately 20 µm, and the average nucleation distance is approximately 2 µm. It was found by experiment that $\beta$ particles break up and transform to $\alpha$-particles. Yet, it is not clear how the $\beta$ plate breaks up during the transformation. In our model we propose that the $\beta$ particles break up with the same length as the nucleation distance. This is illustrated in Fig. 1. Figure 1(a) shows an initial $\beta$ plate with $\alpha$ nuclei. Figure 1(b) shows the situation after a short homogenisation time: The $\beta$ plate breaks up, and the $\alpha$ particles starts to grow. The domain of computation is indicated by the dotted box.

Figure 2 shows the geometry of the model that mimics the growth of an $\alpha$-particle on a dissolving $\beta$-plate. In the FE-Model we calculate an area with the size of $l_{\mathrm{cell}} \times l_{\mathrm{cell}}$. We assume cylindrical symmetry around the left vertical axis. A hemispherical $\alpha$ particle is situated on top of the plate-like $\beta$ particle, and has a distance towards the rim of the $\beta$ particle. The drawing is only schematic as the dimensions are not properly scaled according to those used in the calculations.

The aluminium phase is indicated in Fig. 2 by the domain $\Omega(t)$, in which diffusion of the alloying elements takes place. The time dependence of this domain is induced by the moving boundaries of the $\alpha$-particle and the $\beta$-plate. Those moving boundaries are expressed by the segment CF, defined as $S_{\alpha}$, and the line segment GJ, defined as $S_{\beta}$. The unit normal vectors at the interfaces $S_{\alpha}$ and $S_{\beta}$, pointing outward from the aluminium matrix are denoted by $\boldsymbol{n}_{\alpha}$ and $\boldsymbol{n}_{\beta}$ respectively.

Line segment HK represents a symmetry line. Therefore the presented thickness of the $\beta$-plate in Fig. 2 is only half of the modelled thickness of the $\beta$-plate, $d$. During this

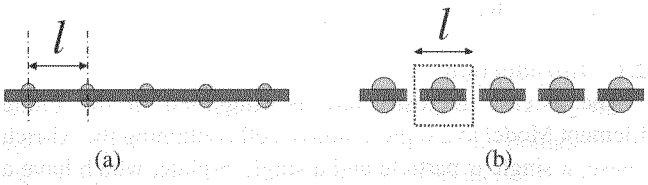


Fig. 1 A scheme of (a) an $\beta$ plate with initial $\alpha$ nuclei in the non-homogenised state (b) A broken $\beta$ plate with consisting $\alpha$ particles on top. The domain of computation is situated in the picture.

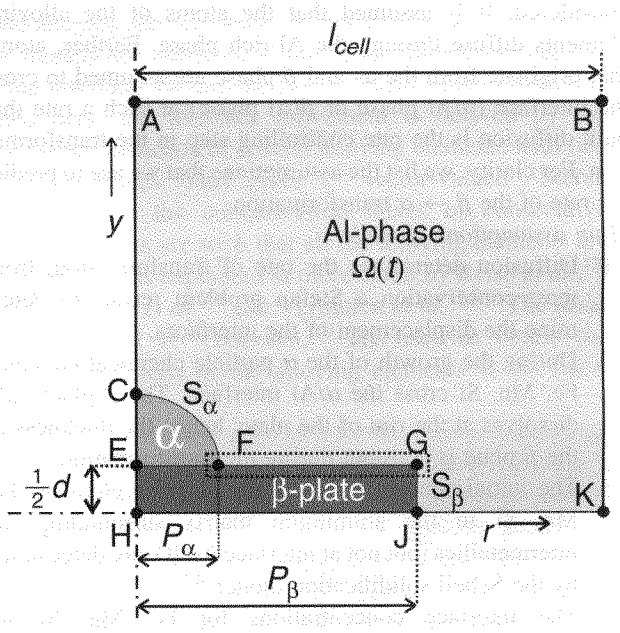


Fig. 2 The geometry of the domain of computation of an $\alpha$-particle on a $\beta$-plate in an Al-phase. The parameters are explained in the text.

transformation this thickness remains constant, as also stated in assumption 1. Line segment AH represent the second symmetry line. For the Finite Element model, cylindrical coordinates are used, where the $\alpha$-particle represents an hemispherical shape and the $\beta$ plate represents a disc like shape in three dimensions.

### 2.4 The finite element model

In this section we present the Finite Element Model for dissolution of the $\beta$-plate and the growth of the $\alpha$-particle which is based on the diffusion of iron only. The boundary conditions at the moving interfaces are determined from solution of eqs. (2) and (3) as described in Section 2.3. In the aluminium matrix, $\Omega(t)$, volume diffusion of iron is modelled by the non-steady state Fick-diffusion equation:

$$\frac{\partial c}{\partial t} = D_{\mathrm{Fe}} \nabla^2 c \quad \text{for} \quad (r, y) \in \Omega(t), \quad t > 0. \tag{4}$$

Here $c$ represents the Fe concentration of iron in the aluminium phase. $t$ is the time of the homogenisation in seconds. From a local mass-balance of Fe over the interfaces, the equation of motion of the interface $S_\alpha$ and $S_\beta$ is derived, leading to a Stefan condition. Let $v_\alpha(t)$ and $v_\beta(t)$ represent the velocity component perpendicular to the interface of the $\alpha$ and the $\beta$ particle, respectively, then:

$$(c_i^{\mathrm{p}} - c_i^{\mathrm{s}}) v_i(t) = D_{\mathrm{Fe}} \frac{\partial c}{\partial n_i} \quad \text{for} \quad (r, y) \in S_i(t), \quad i = \alpha, \beta. \tag{5}$$

The boundary of $\Omega(t)$ is divided into $\Gamma_N(t)$, $S_\alpha(t)$ and $S_\beta(t)$. The part $\Gamma_N(t)$ consists of the cell boundary (line segment CABKJ of Fig. 2) through which we assume no diffusive transport for iron and the non-moving part of the $\beta$-plate (line segment FG of Fig. 2), through which we assume no diffusive transport of iron either. On the boundaries $S_\alpha$ and $S_\beta$ the equilibrium concentrations $c_\alpha^{\mathrm{s}}$ and $c_\beta^{\mathrm{s}}$ are determined from eqs. (2) and (3) and hence they are prescribed in the Finite Element Model.

The presented mathematical problem has been implemented in the package SEPRAN, which has been developed at the Department of Applied Mathematical Analysis at the Delft University of Technology. The resulting Stefan problem is solved by the use of a moving grid method, where the grid is adjusted according to the interface movement. The interface movement is determined in a conservative way. The method is described in detail by Segal *et al.*[30]

In the calculations it is assumed that the initial $\alpha$-particle is spherical with radius $r_\alpha^{\mathrm{init}}$ and that the initial $\beta$-plate is cylindrical with radius $l$. The Gibbs-Thomson effect only has a significant influence on the transformation kinetics when the radius of curvature is very small (typically in the order of nanometer). Since we consider only transformation behaviour in a micrometer-scale, we neglect the Gibbs-Thomson effect in the computations.

## 3. Experimental

An Al–Mg–Si alloy (AA 6005 A) with an alloy composition of 0.70 mass% Mg, 0.83 mass% Si, 0.27 mass% Fe, and 0.18 mass% Mn has been used for our investigations. All other chemical elements were present in weight percentages of at most 0.01 mass%, hence their presence is ignored. The investigated alloy was DC-cast with a diameter of 254 mm respectively.

To investigate the $\alpha \rightarrow \beta$ transformation rate, series of samples were homogenised at temperatures of 540°C, 570°C and 580°C for various times ranging between 10 minutes and 1 day. The samples were homogenised in an air circulation oven, for which the maximum temperature deviation over all locations in the oven is 3°C. The samples were taken from the billet at locations between 10 mm and 30 mm from the rim of the billet. The microstructure of these samples, represent the typical microstructure of the billet. The experimental relative $\alpha$-fraction was determined by using automatic SEM measurements in combination with Electron Dispersive X-ray Spectography (EDX). The $\alpha$- and $\beta$-particles are classified by the difference of stoichiometric ratio of the total concentration of Fe and Mn versus the concentration of Si, which is determined by EDX. The method is described in more detail in 7).

At different distances of 20 mm, 50 mm and 75 mm from the rim of the billet, the mean dendrite arm spacing (DAS) has been determined. Each DAS value was determined by averaging 50 separate DAS-spacings determined from 5 optical micrographs on the same polished sample.

The samples were polished with 1/4 silica and subsequently electro-etched at 20 V during 30 seconds in a mixture of 78 perchloric acid, 90 mL water, 730 mL ethanol and 100 mL butylglycol. SEM micrographs (JEOL 6500F) of these samples were used to measure the mean thickness of the $\beta$-plate. The thickness of the $\beta$-plates was determined by the use of SEM micrographs by averaging 50 individual thicknesses. The true thickness in 3D was taken to be $\pi/4$ times the average thickness from the cross sections images.

The nucleation distance between individual $\alpha$ particles was measured on two fully homogenised samples, either homogenised for 32 hours at 590°C, or homogenised for 130 hours at 540°C. Each sample was polished with 1/4 Silica. Subsequently 20 optical micrographs were made on each sample. The distance between neighbouring $\alpha$ particles ($l$), which were located along a former $\beta$-plate, was determined by the use of the sketch of Fig. 3. The nucleation distance in polished plain is obtained from $L/(n-1)$, where $L$ represents the distance between the outside particles, and $n$ is the number of particles on a sequence. The median nuclei distance, was determined by the use of 20 measurements of $\alpha$-particles. The true nuclei distance in 3D, $l$, was taken to be 1/2 times the median nuclei distance from the measurements.

## 4. Results and Discussion

### 4.1 Introduction

In this section, first a parameter study using the FEM model will be given. Then, the experimental results will be compared with the results obtained by the mathematical models. Finally the metallurgical implications will be given.

As a basis for the model calculations, parameters are used which are deduced from the actual alloy. Most of the simulations are done for an industrial temperature of 580°C, therefore the reported parameters are also obtained for this

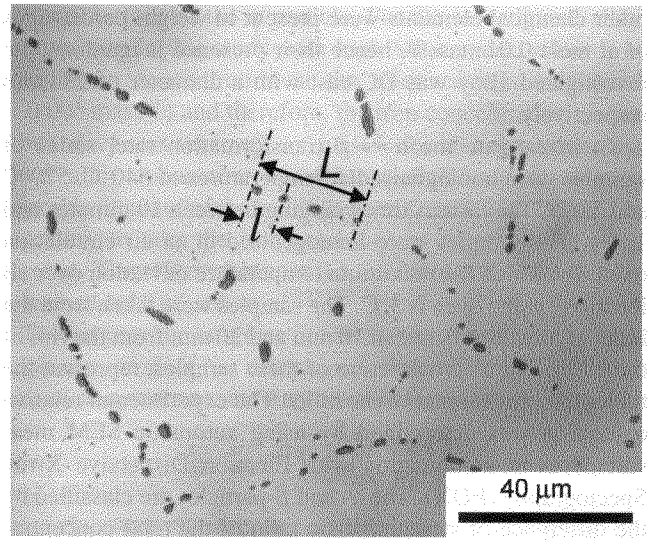


Fig. 3 Microstructure of the fully homogenised sample at 590°C. The method of the determination of the distances between the beads of the $\alpha$ particles on the former $\beta$ plate is showed.

Table 1 Basic physical parameters used for the model.

| Parameter | Symbol | Value |
|---|---|---|
| Diffusion coefficient (at $T = 580$°C) | $D_{Fe}$ | 0.0307 μm$^2$/s |
| Fe concentration in $\alpha$ particle[31] | $c_\alpha^p$ | 39.9 mass% |
| Fe concentration in $\beta$ particle[31] | $c_\beta^p$ | 33.9 mass% |
| Fe content on interface of $\alpha$ particle | $c_\alpha^s$ | 0 mass% |
| Fe content on interface of $\beta$ particle | $c_\beta^s$ | 0.0183 mass% |
| Initial radius of $\alpha$ particle | $r_\alpha^{init}$ | 0.25 μm |
| Thickness of $\beta$-plate | $d$ | 0.2 μm |
| Diameter of initial $\beta$-plate | $l$ | 3 μm |
| Cell size of aluminium matrix | $l_{cell}$ | 2.5 μm |
| Initial iron concentration in matrix | $c_{Fe}^0$ | 0.0200 mass% |
| Temperature | $T$ | 580°C |

temperature (See Table 1). We used the literature values of the densities of Al, $\alpha$ and $\beta$ phases[31] for the derivations of the concentration of Fe inside the $\alpha$ and $\beta$ particles.

The Scheil[26,29] model derives the initial concentration of different elements in the Al-matrix close to the intermetallics. Since the FEM cell is relative small compared to the DAS, and is situated close to the intermetallics, it is assumed that the initial concentration is homogeneously distributed in this FEM cell and is equal to the derived concentrations. By Scheil calculations in Thermo-Calc, which use the compositions of the experimental alloy as input, initial concentrations were found of $c_{Fe}^0 = 0.02$ mass%, $c_{Mg}^0 = 0.6$ mass%, $c_{Si}^0 = 0.5$ mass% and $c_{Mn}^0 = 0.25$ mass%.

The concentrations on the interface of the $\beta$ particles are determined by the multi-component model of eqs. (2) and (3). The geometric parameters, as presented in Table 1, are estimations from previous research.[4,12]

## 4.2 Parameter study using the FEM model

The influence of the physical parameters on the transformed fraction during time is investigated. Here the relative fraction of the $\alpha$ particles with respect to the total amount of intermetallics, is of special interest, since this is an indication of the extrudability of the material, and can also be compared with measurements from experiments. The relative $\alpha$-fraction, $f_\alpha$, is defined as:

$$f_\alpha := \frac{Volume(\alpha)}{Volume(\alpha) + Volume(\beta)}, \tag{6}$$

where $Volume(\alpha)$ is the volume of the $\alpha$ intermetallics and $Volume(\beta)$ is the volume of the $\beta$ intermetallics. Since the model is set up for transformations in the early state, it will only be used until the $\alpha$-particle reach the rim of the $\beta$ particle. Investigations will be performed on the influence on the $\alpha$-fraction by variation of the geometry of the $\alpha$-particle, variation of the geometry of the $\beta$ particle, variation of the matrix, and variation of the temperature.

### 4.2.1 Variation of the size of the $\alpha$ particle

In Fig. 4 the relative $\alpha$-fraction as a function of time, for some modelled microstructures with different initial radii of the $\alpha$ particle is plotted. For all other model parameters, the values are used as presented in Table 1. The presented $\alpha$ radii cover the range of observed $\alpha$ particle sizes on $\beta$ particles as observed in earlier research.[12] The figure shows that the effect of the initial particle size is significant. By the nature of the definition of the relative $\alpha$-fraction $f_\alpha$, a larger initial particle radius gives already a larger initial relative $\alpha$-fraction in the cast condition ($t = 0$). Although the initial $\alpha$-volumes vary widely in this numerical experiment, the $\alpha$-fraction at the point of collision is approximately the same for all conditions, and the time to reach this impingement differs relatively slightly.

### 4.2.2 Variation of the $\beta$ particle

The particle size of the intermetallics depends strongly on the solidification conditions. Fast cooling leads for example to thinner $\beta$ particles. To show its effect on the homogenisation, in Fig. 5 the relative $\alpha$-fraction as function of time is plotted for several values of thickness of the $\beta$-AlFeSi plate. For all other parameters values as in Table 1 are used. Figure 5 shows that with a thin $\beta$ plate already have an initially higher relative $\alpha$-fraction (A larger plate thickness gives a larger initial plate volume and hence the initial relative $\alpha$-

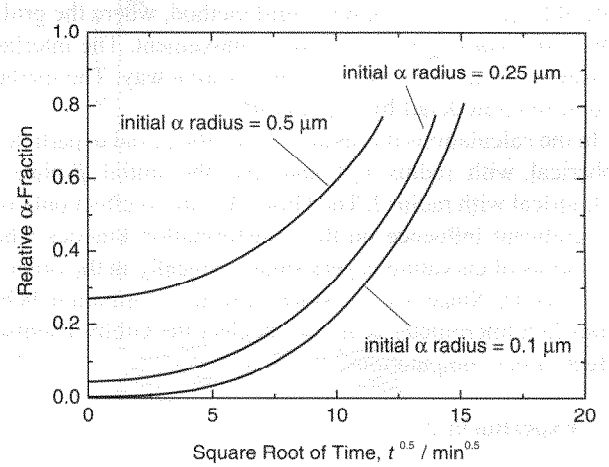


Fig. 4 The relative $\alpha$-fraction as a function of time for different initial particle radii, as computed by the Finite Elements Model. The other model parameters are presented in Table 1.

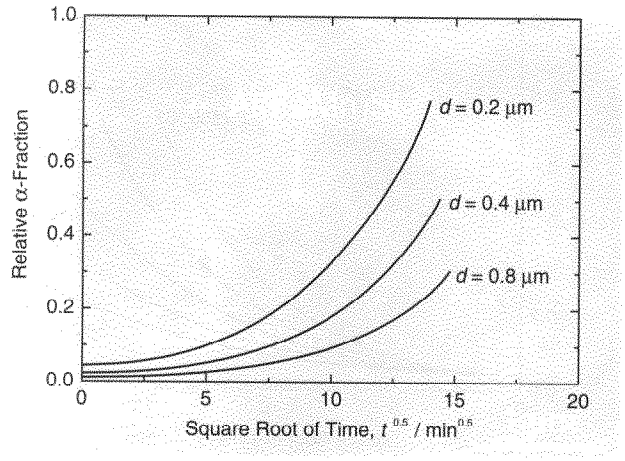


Fig. 5 The relative α-fraction as a function of time for consecutive β-plate thicknesses, as computed by the Finite Elements Model. The other model parameters are presented in Table 1.

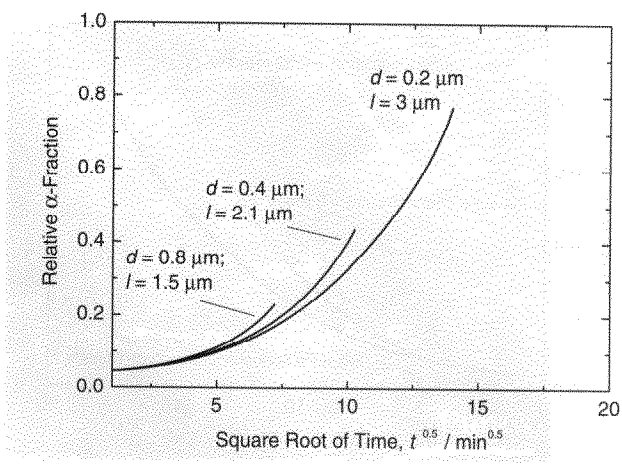


Fig. 7 The relative α-fraction as a function of time for consecutive aspect ratio's of the β plate, as computed by the Finite Elements Model. The consecutive thicknesses ($d$) and diameters ($l$) of the β plates are indicated in the graph. The other model parameters are presented in Table 1.

fraction is smaller). Figure 5 also shows that the time of impingement is approximately the same for all β thicknesses. Therefore the velocity of the movement of the α to the β must be approximately equal for all cases. On the other hand, the relative α-fraction at impingement is highly dependent on the β-thickness.

In Fig. 6 the relative α-fraction as a function of time is given for several values of the initial radius of the β plate. This radius can be interpreted as the nucleation distance between the α particles, and therefore the average distance of the α plate towards the rim of the β plate. Again, the figure shows that the effect of the size of the β plate on the transformation is significant. Figure 6 shows that, as induced by the definition of the relative α-fraction, situations with a large initial radius gives a small initial relative α-fraction. The time of impingement is strongly dependent of the initial β plate radius. Smaller β plates impinge earlier, which is clearly visible in the figure. Also the relative α-fraction of impingement is higher as the initial β plate becomes larger.

In Fig. 7 the relative α-fraction as function of time is plotted for several values of the aspect ratio of the β plate, such that the initial volume of the β plate is the same for all curves. It can be seen that the influence of the initial β-plate thickness and initial β-plate radius compensate each other, and therefore the relative α fraction during time is almost equal. As may be expected from the assumptions, the collision time of the α particle and the β rim increases considerably for larger β-plate radii and the model breaks down at a later stage.

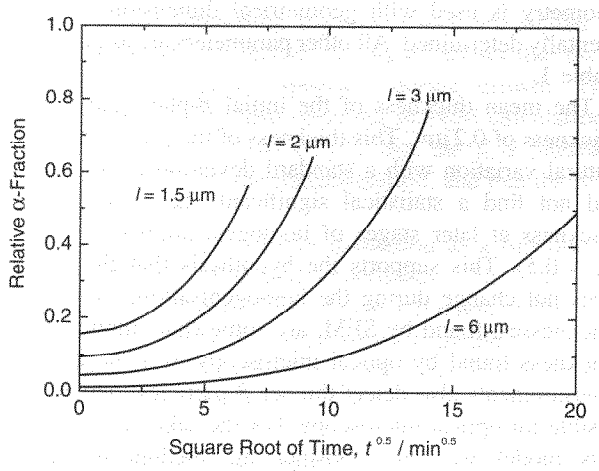


Fig. 6 The relative α-fraction as a function of time for consecutive initial β-plate radii, as computed by the Finite Elements Model. The other model parameters are presented in Table 1.

### 4.2.3 Variation of the matrix

Calculations with different cell sizes reveal that the influence of the cell-size on the transformation rate is not significant. The results of these computations are not shown here. We conclude that the cell-size hardly influences the transformation kinetics.

The used cell-size is correlated to the DAS of an alloy. Since the measured DAS spacing of most of the 6xxx alloys are in the order of 20 μm, thus larger than the β-plate sizes, it can be concluded that variations in the DAS have little influence on the transformation speed of the intermetallics.

The Scheil-model on the AA 6005A alloy composition gives an initial iron concentration of $c^0_{Fe} = 0.02$ mass% close to the β-AlFeSi intermetallics. Since the Scheil model is based on ideal solidification, it is useful to investigate the effect of other initial solute iron concentrations. Figure 8 present the relative α-fraction as a function of time for several values of the initial iron concentration in the Al-matrix. The figure shows that cases with initial iron concentrations between 0 and 0.02 mass% Fe give approximately the same kinetics. A higher initial Fe concentration, of 0.05 mass% will slow down the transformation. In this case, the initial Fe concentration in the Al-matrix exceeds the solubility on the rim of the plate, leading to an initial growth rather than shrinkage of the β plate. Although this effect seems unrealistic in 6xxx alloys, growth of β plates has been observed in other alloy systems.[32]

### 4.2.4 Variation of temperature

Figure 9 shows the $\beta \rightarrow \alpha$ transformation as computed for various temperatures. The input conditions for the various temperatures are taken from Table 1. Both the solubility at the interface ($c^s_{\beta Fe}$) and the diffusion coefficients of the

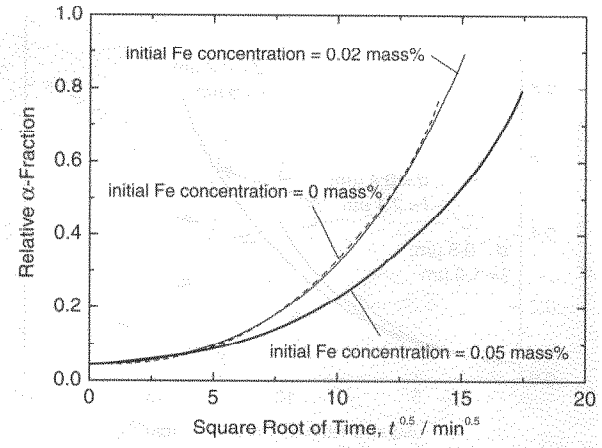


Fig. 8 The relative $\alpha$-fraction as a function of time for consecutive initial Fe concentrations in the Aluminium matrix, as computed by the Finite Elements Model. The other model parameters are presented in Table 1.

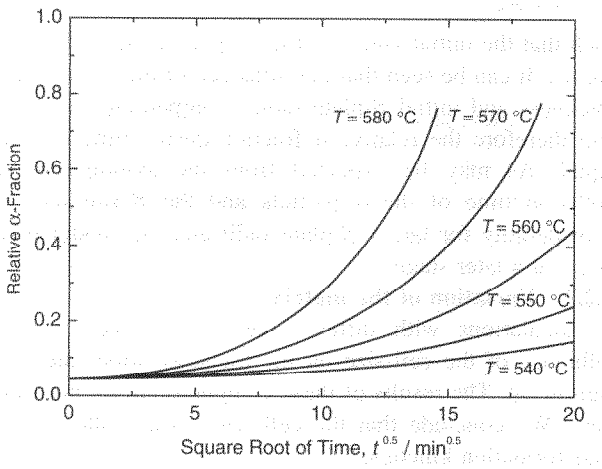


Fig. 9 The relative $\alpha$-fraction as a function of time for consecutive homogenisation temperatures, as computed by the Finite Elements Model. In the derivations, both the temperature dependence of the iron solubility concentration on the interface, and the diffusion coefficient of iron is taken into account, which parameters are presented in Table 2. The other model parameters are presented in Table 1.

chemical elements are functions of temperature. By using the multi-component model and solubility product (eqs. (2) and (3)), the solubility on the interface can be calculated and results are listed in Table 2 for the relevant temperatures. As was discussed in Section 2.2, the table shows that the main difference in solubility is in $c^s_{\beta\mathrm{Fe}}$ and the solubility of silicon approximately equals the concentration of the matrix, *i.e.* $c^s_{\mathrm{Si}} \approx c^0_{\mathrm{Si}}$. For the calculations of the solubility, the Arrhenius relation of the diffusion coefficient is used with pre-factor of $D_{0\mathrm{Si}} = 2.02 \cdot 10^{-4}\,\mathrm{m^2 s^{-1}}$ and activation energy $Q_{\mathrm{Si}} =$

Table 2 Input data for the computations at consecutive temperatures.

| Physical quantity | $T = 540°C$ | $T = 570°C$ | $T = 580°C$ |
|---|---|---|---|
| $c^s_{\beta\mathrm{Fe}}$ (mass%) | 0.00850 | 0.0152 | 0.0183 |
| $c^s_{\beta\mathrm{Si}}$ (mass%) | 0.508 | 0.510 | 0.510 |
| $D_{\mathrm{Fe}}$ ($\mu m^2 s^{-1}$) | 0.00861 | 0.0226 | 0.0307 |
| $D_{\mathrm{Si}}$ ($\mu m^2 s^{-1}$) | 0.369 | 0.755 | 0.948 |

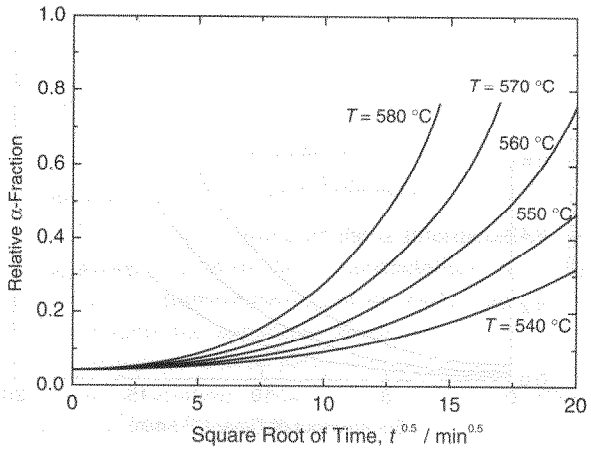


Fig. 10 The relative $\alpha$-fraction as a function of time for consecutive homogenisation temperatures, as computed by the Finite Elements Model. In the derivations, only the temperature dependence of the diffusion coefficient of iron is taken into account, which parameters are presented in Table 2. The other model parameters are presented in Table 1.

123.9 kJ/mol for the diffusion of Silicon,[28] and pre-factor $D_{0\mathrm{Fe}} = 5.3 \cdot 10^{-3}\,\mathrm{m^2 s^{-1}}$ and activation energy $Q_{\mathrm{Fe}} =$ 183.4 kJ/mol for the diffusion of iron.[33]

Figure 9 shows that the transformation kinetics are highly temperature dependent. An increase of *e.g.* 25°C of the temperature can increase the transformed state considerably. This rapid increase is caused by two effects: both the solubility at the rim, and the diffusion coefficient increases with increasing temperature. To illustrate the effect of increasing temperature, without the influence of the solubility, calculations are performed with a fixed solubility of $c^s_{\beta\mathrm{Fe}} = 0.0183$ mass%. The results are plotted in Fig. 10. In this case, the temperature has significantly less effect on the transformation speed than for the results shown in Fig. 9, as is to be expected.

### 4.3 Model versus experiments

In the previous sections, we showed that the model showed realistic characteristics. In this section we want to perform a more quantitative comparison of the model calculations versus experiments. For the model calculations a cylindrical geometry is used with geometrical dimensions as experimentally determined. All other parameters are as presented in Table 1.

The mean thickness of the initial $\beta$-plate had a median thickness of 0.2 µm. This thickness of the $\beta$ plate had a wide natural variation with a standard deviation of 0.15 µm. We did not find a statistical significant change in the mean thickness at later stages of homogenisation ($f_\alpha \approx 0.2$ and $f_\alpha \approx 0.5$). This supports the hypothesis that the thickness does not change during the homogenisation. Note that the thicknesses, found by SEM, are somewhat smaller than the thickness found by optical microscopy in 4) because SEM measurements also detect thinner $\beta$ particles, which are not visible for optical microscopy. For the sake of simplicity, in this model we only consider the median thickness in calculations.

The nucleation distance of the $\alpha$ particles was determined. For the fully homogenised sample at 540°C the median

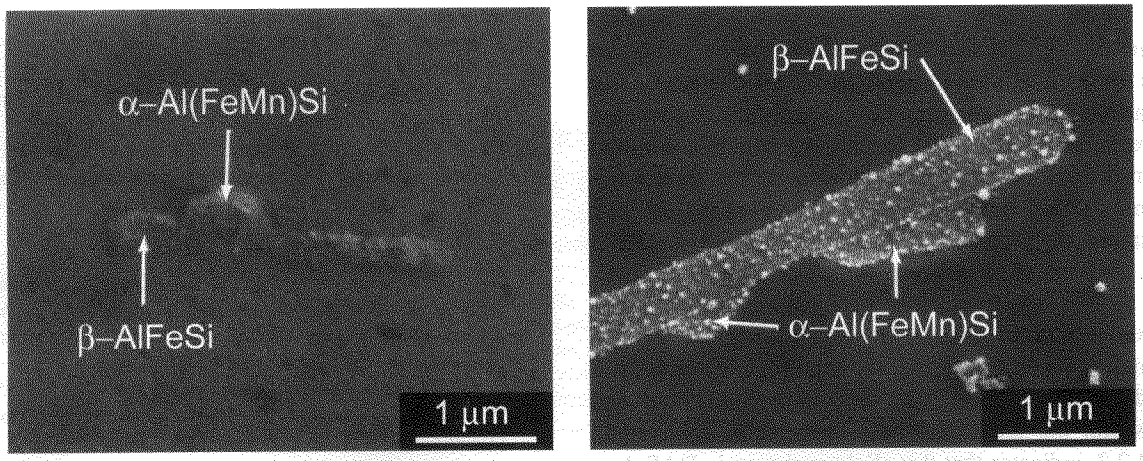


Fig. 11 A micrograph of the Scanning Electron Microscope of an alloy homogenised at 540°C for 2 hours. (a) An α particle on a β particle. (b) Multiple α particles on a β particle.

distance was equal to 1.75 μm, and for a fully homogenised sample at 590°C this distance equals approximately 1.5 μm. There is a wide natural variation of the nucleation distances, with a standard deviation of 0.5 μm, but for the sake of simplicity, in this model we only take the nucleation density $l = 1.5\,\mu m$ as a model parameter, and we neglect the temperature dependence. Note that although this median nucleation distances was corrected for the 3D situation, this values still fall in the measured distribution of the nucleation distances in the 2D plane.

The average DAS was approximately 20 μm. In Section 4.2.3., we found that the cell size does hardly has any influence on the numerical results providing it is larger than the β plate. Therefore, to reduce the computational effort, we used a numerical cell size which is smaller than the dendrite arm spacing, $l_{cell} = 2.5\,\mu m$.

The morphology assumed in the model calculations was also validated against some SEM micrographs. Figure 11(a) shows an SEM micrograph of an α particle which grows on top of a β plate. The morphology of this figure corresponds well to the numerical calculations. Figure 11(b) shows multiple α particles on one β plate. For the sake of simplicity we restrict ourselves in the model to one α particle. However, this figure shows interesting features, which are similar to those in the FE-Model. Firstly, this figure shows that the α particle does not remain spherical during growth. This asymmetrical growth is also observed in FEM calculations. Secondly, this figure shows clearly that the β/α interface remains in place during the transformation, and that the β/Al interface remains flat.

Figure 12 shows the relative α-fraction as a function of time computed by FEM and experiments. The time and temperature dependence of the relative α-fraction of the FEM model agrees well with the experiments. It should be pointed out that the model is capable to predict the transformation fraction up to approximately $f_\alpha = 0.5$.

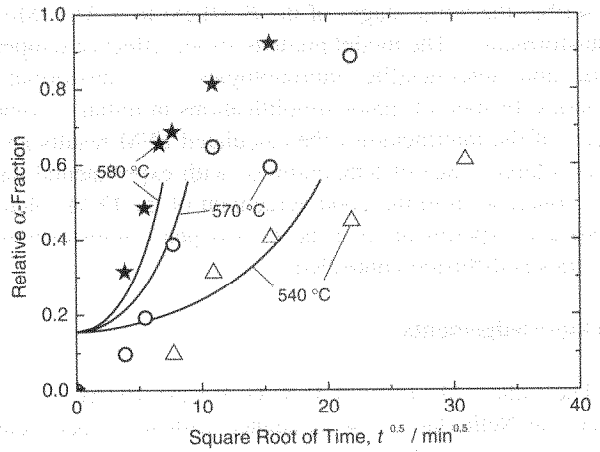


Fig. 12 The relative α-fraction as a function of time derived by the Finite Element Model (presented by the straight lines) compared with the relative α-fractions, measured by experiments (presented by the separate points). The calculations and measurements are performed for three different temperatures.

### 4.4 Metallurgical implications

A proper homogenisation leads to a considerably increase in the extrudability and leads to less surface defects on the aluminium profiles. Therefore, preferably an extrusion ingot is homogenised to attain a high relative α fraction, *e.g.* preferable at least $f_\alpha = 0.8$ and preferably more than $f_\alpha = 0.9$.[1] Although the presented transformation model is not applicable to homogenisation up to high relative α-fractions, yet still some important metallurgical implications can be already extrapolated from the numerical experiments.

Three aspects influences the homogenisation process in particular: the morphology of the intermetallics, the homogenisation temperature, and the alloy content. The influence of the alloy composition was not investigated in this study and will be discussed by Kuijpers *et al.*[25]

A high temperature dependence of the transformation rate was found, both for numerical and experimental results. Industrial homogenisation temperatures of extrusion ingots are typically at approximately 585°C.[1] The model showed that a decrease of the homogenisation temperature of *e.g.* 5°C leads to a considerably increase of the required homogenisation time of ~20%. Therefore, accurate temperature control is a very important aspect to achieve efficient homogenisa-

tion.

The morphology of the intermetallics has an important effect on the transformation speed. Section 4.2 indicates that thin $\beta$-particles will transform faster than thick $\beta$ particles. Therefore it is important that the as-cast structure contains more thin distributed $\beta$ particles, to achieve fast homogenisation times. Grain refiners, alloy composition and cooling speed mainly determines the coarseness of the $\beta$-AlFeSi particles, and therefore those parameters have to be optimised.

Also the effect of the DAS was investigated on the transformation speed. Experiments on the studied AA 6005 A alloy indicates that the DAS ranges between 19 μm and 23 μm, within the DC-cast billet. The results as given in Section 4.2.3. indicates that this slight variation in DAS does not lead to a significant effect on the transformation speed.

## 5. Conclusions

A Finite Element Model has been presented which describes the initial stages of the $\beta$-AlFeSi to $\alpha$-Al(FeMn)Si transformation. The model predicts strong effect of temperature and intermetallic morphologies on transformation kinetics. In spite of major simplifications in initial morphologies of the intermetallics the calculated FEM results agree over a large range of temperatures, with experimental data. We conclude from the good agreement of the FEM calculations and experiments that the $\beta \rightarrow \alpha$ phase transformation kinetics is diffusion controlled.

## Acknowledgements

The authors like to thank P. T. G. Koenis, BOAL B.V., de Lier, the Netherlands, for assistance with the experimental determination of the relative $\alpha$-fractions on homogenised samples, C. Kwakernaak and J. Kiersch of the Delft University of Technology, the Netherlands, for assistance with the JEOL 6500F, J. P. Mulder, Aluminium Delfzijl, Delfzijl, the Netherlands, for the determinations of the DAS, and S. Leever, student at the Delft University of Technology, the Netherlands, for the measurements on the nucleation distances of the $\alpha$-particles. This research was carried out under project number MP 97009-3 in the framework of the strategic research program of the Netherlands Institute for Metals Research in the Netherlands (www.nimr.nl).

## REFERENCES

1) N. C. Parson, J. D. Hankin and K. P. Hicklin: *Al–Mg–Si alloy with good extrusion properties*, US-pattent (2002) 6,440,359.
2) S. Zajac, B. Hutchinson, A. Johansson and L. O. Gullman: Mater. Sci. Tech. **10** (1994) 323–333.
3) A. Valles, R. P. L. Orsetti and R. Tosta: Proc. of the International Conference on Aluminium Alloys, (Toyohashi, Japan, 1998) 2123–2128.
4) N. C. W. Kuijpers, J. Tirel, D. N. Hanlon and S. van der Zwaag: Mater. Char. **48** (2002) 379–392.
5) M. P. Clode and T. Sheppard: Aluminium Technology '86, (The Institute of Metals, 1 Carlton House Terrace, London SW1Y 5DB, UK, 1986) pp. 230–239.
6) T. Minoda, H. Hayakawa and H. Yoshida: Mater. Sci. Technol. **7** (2000) 13–17.
7) N. C. W. Kuijpers, W. H. Kool, P. T. G. Koenis, K. E. Nilsen, I. Todd and S. van der Zwaag: *Assessment of different techniques for quantification of intermetallics in AA 6xxx alloys*, accepted for publication in Mat. Charact. 2003.
8) S. Onurlu and A. Tekin: J. Mater. Sci. **29** (1994) 1652–1655.
9) H. Tanihata, T. Sugawara, K. Matsuda and S. Ikeno: J. Mater. Sci. **34** (1999) 1205–1210.
10) H. J. Lamb: Proc. of the Conf. on Phase Transformations, (London, England, 1979) Series 3, No. 1, 2, V4-V5.
11) L. Lodgaard and N. Ryum: Mater. Sci. Eng. A **283** (2000) 144–152.
12) N. C. W. Kuijpers, J. Tirel, D. N. Hanlon and S. van der Zwaag: *On the characterisation of the α-Al(FeMn)Si nuclei on β-AlFeSi intermetallics by Laser Scanning Confocal Microscopy*, send for publication in J. of Mater. Sci. Lett.
13) N. C. W. Kuijpers and S. v.d. Zwaag: "*Observations of α-Al(FeMn)Si nuclei on β-AlFeSi intermetallics by SEM*", to be send for publications in J. of Mater. Sci.
14) J. Crank: *Free and moving boundary problems*, (Clarendon Press, Oxford, 1984).
15) M. J. Whelan: Metal. Sci. J. **3** (1969) 95–97.
16) H. B. Aaron and G. R. Kotler: Metall. Trans. A **2** (1971) 393–408.
17) U. H. Tundal and N. Ryum: Metall. Trans. A **23** (1992) 433–444.
18) O. Reiso, J. Strid and N. Ryum: Metall. Trans. A **24** (1993) 2629-41.
19) R. Hubert: ATB Metallurgie **34–35** (2002) 4–14.
20) J. M. Vitek, S. A. Vitek and S. A. David. Metall. Trans. A **26** (1995) 2007–2025.
21) F. J. Vermolen and C. Vuik. J: Comput. Appl. Math. **126** (2000) 233–254.
22) F. J. Vermolen, C. Vuik and S. van der Zwaag: Mater. Sci. Eng. A **328** (2002) 14–25.
23) R. Kobayashi: Physica D **63** (1993) 410-23.
24) U. Grafe, B. Bottger, J. Tiaden and S. G. Fries: Scr. Mater. **42** (2000) 1179-86.
25) N. C. W. Kuijpers, P. T. G. Koenis, K. E. Nilsen, F. Vermolen, C. Vuik and S. v. d. Zwaag: "*Alloy dependence of the β-AlFeSi to α-Al(FeMn)Si transformation kinetics in Al–Mg–Si alloys*", to be submitted to Mater. Trans., 2003.
26) E. Scheil: Z. Metallkd **34** (1942) 70–72.
27) D. T. L. Alexander and A. L. Greer: Acta Mater. **50** (2002) 2571-83.
28) S. Fujikawa, K. I. Hirano and Y. Fukushima: Metall. Trans. A **9** (1978) 1811–1815.
29) D. A. Porter and K. E. Easterling: *Phase transformations in Metals and Alloys*, (Chapman & Hall, London, 1997).
30) G. Segal, C. Vuik and F. J. Vermolen: J. Comp. Phys. **141** (1998) 1–21.
31) L. F. Mondolfo: *Structure and Properties of Aluminium Alloys*, (Butterworth, England, 1976).
32) N. A. Belov, A. A. Aksenov and D. G. Eskin: *Iron in Aluminum Alloys. Impurity and Alloying Element*, (Taylor & Francis, Londen and New York, 2002) 132–136.
33) D. L. Beke, I. Gödény, I. A. Szabó, G. Erdélyi and F. J. Kedves: Philos. Mag. A **5** (1987) 73–78.